Multiaxial fatigue life prediction for a natural rubber

Nicolas Saintier, Georges Cailletaud, Roland Piques

▶ **To cite this version:**

Nicolas Saintier, Georges Cailletaud, Roland Piques. Multiaxial fatigue life prediction for a natural rubber. International Journal of Fatigue, 2006, 28 (5-6), pp.530-539. 10.1016/j.ijfatigue.2005.05.011 . hal-00145066

HAL Id: hal-00145066
https://hal.science/hal-00145066

Submitted on 28 Sep 2017

HAL is a multi-disciplinary open access archive for the deposit and dissemination of scientific research documents, whether they are published or not. The documents may come from teaching and research institutions in France or abroad, or from public or private research centers.

L'archive ouverte pluridisciplinaire **HAL**, est destinée au dépôt et à la diffusion de documents scientifiques de niveau recherche, publiés ou non, émanant des établissements d'enseignement et de recherche français ou étrangers, des laboratoires publics ou privés.

Multiaxial fatigue life prediction for a natural rubber

N. Saintier [a,b,*], G. Cailletaud [b], R. Piques [b]

[a] *LAMEFIP, Ecole Nationale Supérieure des Arts et Métiers, Esplanade des Arts et Métiers, 33405 Talence cedex, France*
[b] *Centre des matériaux P.M. FOURT, Ecole Nationale Supérieure des Mines de Paris, UMR CNRS 7633, 91003 Evry cedex, France*

This study deals with the fatigue crack initiation under multiaxial non-proportional loadings in a natural rubber. Push–pull, torsion and tension-compression with a superimposed static torsion fatigue test results are presented. A short presentation of some important features concerning short fatigue crack growth is given. Two fatigue crack criteria are proposed, the first one based on the first and second invariant of the Cauchy stress tensor, the second, based on the micromechanisms of crack initiation, consist of a critical plane approach under large strain conditions using a micro to macro approach. The second criterion was found to give the best results, by predicting the fatigue lifes, crack orientations and location, even in cases with internal crack initiation.

Keywords: Multiaxial fatigue; Natural rubber; Crack initiation; Fatigue life prediction; Critical plane approach; Large strain

1. Introduction

Cut growth studies on natural rubber (NR) have been reported by many authors [1–3]. Most of these studies are dealing with precracked specimens and correlate the crack growth with the fracture energy. Fewer studies are dealing with fatigue crack initiation in unprecracked specimens even though it is the case in practice. In comparison to metallic materials and despite their growing use in a wide range of industrial applications, elastomers have been very little considered by researchers working on fatigue life prediction under complex loadings. Appropriate fatigue life criteria are needed by engineers to prevent their failure in service. In a recent review, Mars [4] emphasis the lack of adequate multiaxial fatigue life criteria for elastomers. Moreover, the underlying mechanisms of the very first stage of crack initiation and propagation are rarely discussed. The aim of this paper is to present briefly the characteristics of the very first stage of crack propagation (an extensive study of those mechanisms can be found in [5]) and to propose a multiaxial fatigue life criterion for rubber.

* Coressponding author. Adderss: LAMEFIP, Ecole Nationale Supérieure des Arts et Métiers, Esplanade des Arts et Métiers, 33405 Talence cedex, France.
E-mail address: nsaintie@lamef.bordeaux.ensam.fr (N. Saintier).

2. Material and mechanical testing

The elastomer used in the present study was a vulcanized natural rubber material (NR) filled with 23 parts of reinforcing carbon black (N772, N330) per hundred part of rubber. The molecular structure consist of *cis* − 1,4-polyisoprene chains. This particular *cis*- configuration allow the molecular chains to crystallize under tension. The minimum strain level necessary to induce this phase transformation was identified using X-ray diffraction and was found to be around 130% (see [5] for more details on the procedure). Formulation and basic mechanical properties are given in Table 1. Fatigue tests were carried out at room temperature on three types of specimens (see Fig. 1), all molded by injection. The elastomer was bonded to the metal end pieces during the vulcanization process. Diabolos are almost uniaxial specimens when carrying out push–pull testing (triaxiality 0.34) whereas axisymmetrical notched (AN) specimens show triaxiality between 0.55 (AN2) and 0.45 (AN5) depending on the notch radii.

Fatigue testing was performed using push–pull and torsion home made electromechanical fatigue machines. Fatigue machines were supplied with waveforms generated by a digital-to-analogue converter under PC control. Number of cycles, force and displacement data were recorded by the PC via an analogue-to-digital converter. All tests were carried out at room temperature and at low frequency (1 Hz). Push–pull and torsion tests were conducted on Diabolo, AN2 and AN5

Table 1
Room temperature mechanical properties

Density (g/m^3)	A shore hardness	*UTS* (MPa)	ϵ_{fail} (%)	300% Elong. modulus (MPa)
1.1	48	25.3	500	7.8

specimens at various loading ratios. Push–pull tests with a superimposed static torsion were also performed on Diabolos. Those tests are particularly interesting as they show systematic internal crack initiation. The mechanisms responsible for such internal initiations are very different from those observed in metalic materials. The ability of the proposed criterion to locate correctly the crack initiation in those cases is critical and will be considered as good indicator of the quality of the predictions.

Fatigue tests were conducted at least to crack initiation, and in most cases to rupture. The number of cycles to crack initiation N_i is conventionally defined as the number of cycles necessary to obtain a crack of 1mm size wherever in the tested specimen. N_i is difficult to determine unambiguously since neither compliance changes nor potential drop technique can be used with those materials. In order to detect the appearance of fatigue cracks, the specimen surface was observed during the test at regular time intervals, using an optical microscope. N_i was reached as soon as a 1 mm crack was observed.

The uniaxial data base includes more than 80 tests results on diabolos (including 40 of a previous study done at the laboratory [6]) with fatigue lives ranging from 0.3×10^5 to 10^6 cycles. The number of specimens could be considered as low compared to fatigue life prediction studies on metallic materials but at the frequencies considered (1 Hz) this represents a cumulated testing time of 11,000 h which is equivalent to test 2400 specimens at 60 Hz and 10^6 cycles.

3. Numerical procedure

Rubbery materials are well known for having complex behaviors including stress softening, hysteresis and non-linearity effects. For natural rubber the hysteresis behavior appears at high strains (above 200–250%) and is generally attributed to a phase transformation process (crystallisation). Fatigue tests were conducted at maximum strains of 100% so that the hysteresis part of the behavior was not considered in the modeling. Stress softening effects appear at low strain levels. When considering a structure, the local (i.e. on one point of the structure) stress softening, also called the Mullins effect [7], is depending non-linearly on the local first principal maximal strain ϵ_{max} reached during the cycle (see [8] for experimental results and numerical modeling on SBR). However, for our material, in the strain range investigated in this study, the stress softening effect was showing sufficiently low dependency on ϵ_{max} to be considered as constant. Then, the behavior was identified on a stabilized material at an elongation equal to the maximum elongation reached during the fatigue tests.

A largely used model for rubbers is the Mooney–Rivlin model which includes large strain formulation and non-linear description of the stress-strain relation. The strain tensor in the actual configuration noted $\underset{\sim}{\mathbf{A}}$ (also called the Euler–Almansi tensor), is expressed as follow:

$$\underset{\sim}{\mathbf{A}} = \frac{1}{2}(\underset{\sim}{\mathbf{I}} - \underset{\sim}{\mathbf{B}}^{-1}) \tag{1}$$

with $\underset{\sim}{\mathbf{B}} = \underset{\sim}{\mathbf{F}}\underset{\sim}{\mathbf{F}}^{-1}$ the left Cauchy-Green tensor. In the initial configuration, the so-called Green-Lagrange strain tensor $\underset{\sim}{\mathbf{E}}$ is expressed as follow:

$$\underset{\sim}{\mathbf{E}} = \frac{1}{2}(\underset{\sim}{\mathbf{C}} - \underset{\sim}{\mathbf{I}}) \tag{2}$$

where $\underset{\sim}{\mathbf{C}} = \underset{\sim}{\mathbf{F}}^t\underset{\sim}{\mathbf{F}}$ is the right Cauchy-Green tensor.

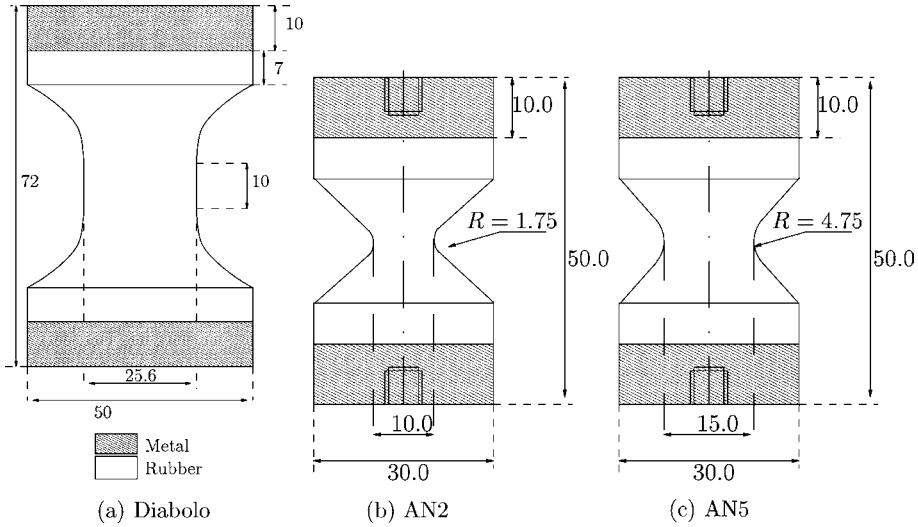

Fig. 1. Specimens geometries used for fatigue tests.

In the actual configuration, the stress tensor is known as the Cauchy stress tensor (real stresses to be taken into account in a stress based fatigue life criteria). Non-linear hyperelastic models are generally based on the formulation of a strain energy density W which is related to the Cauchy stress tensor via the first principle of thermodynamics. The stress tensor is obtained by differentiating the strain energy function with respect to the left Cauchy-Green tensor $\underset{\sim}{\mathbf{B}} = \underset{\sim}{\mathbf{F}}\underset{\sim}{\mathbf{F}}^t$ as follow:

$$\underset{\sim}{\mathbf{T}} = 2\rho\underset{\sim}{\mathbf{B}}\frac{\partial W}{\partial \underset{\sim}{\mathbf{B}}} \tag{3}$$

where ρ is the density. Unless specified, the term of stress will always refer to Cauchy stress. A simple strain energy formulation was found to give good results in the range of stress, strain and loading frequencies investigated in this study: the Money-Rivlin model. For incompressible materials it is expressed as follow:

$$W(I_1, I_2) = \sum_{i,j=0}^{\infty}(C_{ij}(I_1-3)^i(I_2-3)^j) \tag{4}$$

where W is the strain-energy density and I_1, I_2 are the first two invariants of the Green deformation tensor. For the loading cases encountered in this study, material stress-strain properties were found to be well described by:

$$\begin{aligned} W(I_1, I_2) = {} & C_{10}(I_1-3) + C_{01}(I_2-3) + C_{11}(I_1-3) \\ & \times(I_2-3) + C_{20}(I_1-3)^2 + C_{30}(I_1-3)^3 \end{aligned} \tag{5}$$

3.1. Identification

Material parameters have been identified on experimental load-displacement curves from simple tensile tests on strips of material but also from tension-compression tests on Diabolo specimens using an inverse method. F.E. calculations were coupled to an optimizer to identify material parameters from experimental load-displacement curves. Both F.E. computations and the optimization loop were driven by the F.E. code Zebulon [9] developed at the laboratory. The optimized set of parameters are $C_{10}=0.284$, $C_{01}=0.105$, $C_{11}=0.106\times10^{-2}$, $C_{20}=0.237\times10^{-2}$, $C_{30}=0.104$. An example of an optimized stress-strain curve is given in Fig. 2.

4. Experimental results

4.1. Uniaxial fatigue

More than 80 specimens were tested, with fatigue lives ranging from 3×10^4 to 10^6 cycles. Experimental results obtained on diabolos are presented Fig. 3(a) in an Haigh diagram using the mean and amplitude of axial Cauchy stress. Stress values were calculated at the critical point of the structure (i.e. location of crack initiation). It shows that at negative loading ratios ($R=(\sigma_{\min}/\sigma_{\max})$) the fatigue life decreases as the stress amplitude increases, whereas the tendency is reversed as soon as R becomes positive.

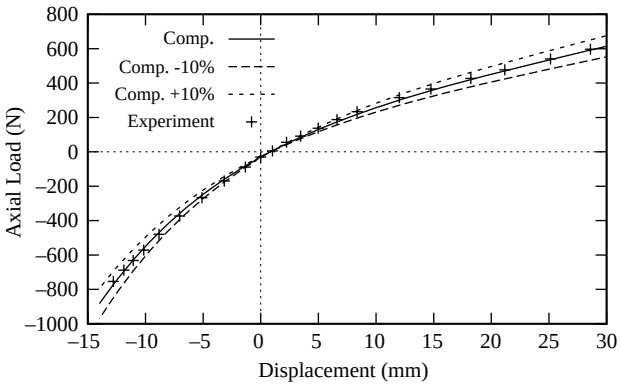

Fig. 2. Comparison between computed and experimental behavior for a tension-compression loading with a superimposed static torsion (80°).

The lifetime contour plots reflect a strong reinforcing effect for $R>0$. Such reinforcing effects have been reported in crack propagation studies by many authors [1,10,11] and has been observed mainly on natural rubber. The mechanisms behind this phenomena will not be fully explained here but can be found in [5]. However it is important to acknowledge that the ability of natural rubber to crystallize under straining plays a major role in the reinforcement. Under uniaxial loadings, it was shown [5] that a process of accumulation of crystallisation takes place in the crack tip region as soon as the minimum axial

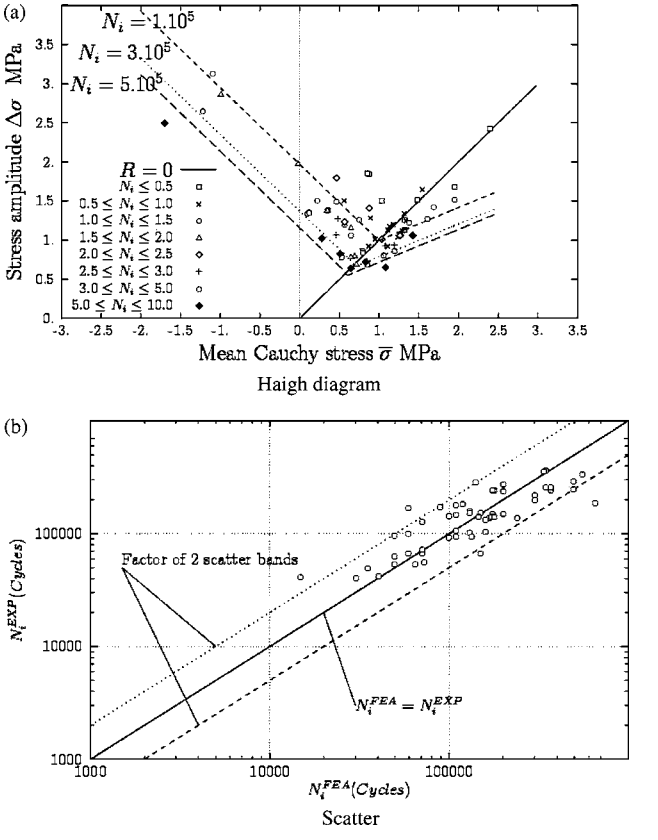

Fig. 3. Uniaxial results plotted in an Haigh diagram using the axial mean Cauchy stress vs. axial Cauchy stress amplitude.

stress reached during a cycle is greater than a critical value (greather than zero). The crystallisation cumulation process induces strong microstructural modifications in the crack tip region, which are responsible for inhibiting part of the crack initiation and propagation damage mechanisms.

4.2. Crack orientations under multiaxial fatigue loading

Under non-proportional multiaxial loading, depending on the type of material, fatigue cracks are found to appear in the direction of maximum shear amplitude (shear cracking), maximum normal stress (tensile cracking) or even mixed mode cracking (shear and tensile cracking). In order to establish which mode is relevant for natural rubber, specimen surfaces were systematically observed using a field effect Zeiss scanning electron microscope (SEM). Cracks orientations have been measured, in the undeformed configuration, and compared to the direction given by the maximum first principal stress reached during a cycle. It has to be noticed that due to large deformations, crack orientations, measured in the undeformed configuration, cannot be directly compared to computed principal stress direction which is computed in the deformed configuration. Indeed, due to large strain conditions, physical planes undergo large rotations, during deformation, over a cycle. Since principal stress direction rotations and physical plane rotations are not the same they can not be directly compared in the undeformed configuration. Computed principal stress directions, in the deformed configuration, have to be transported into the undeformed configuration before comparison with measured crack angles. Details of the calculations will be given in the 'Critical plane approach' section. Finally, a good correlation has been observed between crack orientation and maximal principal stress directions so that under multiaxial loading, NR can be considered as exhibiting tensile mode cracking (see [21] for more details).

5. Fatigue life prediction

5.1. Uniaxial formulation

As said previously, the effect of non-relaxing conditions is to increase very markedly the fatigue life resistance of crystallising rubbers. Due to this reinforcement, it is impossible to apply a simple wohler approach: by using an unique mechanical parameter we are unable to predict such a reinforcement. Two variables are needed to describe the whole experimental data base. Cauchy stress amplitude and mean Cauchy stress were found to be the most relevant parameters. Each test performed under push–pull conditions was plotted in an Haigh diagram ($\Delta\sigma, \bar{\sigma}$). Andre [6] proposed to model the lifetime contour plots by two sets of straight lines in this diagram. The number of cycles to crack initiation (equal to constant along those lines) was correlated to the stress state via a power law function of an equivalent stress (also constant along those lines). The criterion can then be expressed as follows:

$$\sigma_{eq} = \begin{cases} \Delta\sigma + \beta_1\bar{\sigma} & \text{if } R < 0 \\ \beta_2\Delta\sigma + \beta_3\bar{\sigma} & \text{if } R \geq 0 \end{cases} \tag{6}$$

or, in a unified manner:

$$\sigma_{eq} = H(-R)(\Delta\sigma + \beta_1\bar{\sigma}) + H(R)(\beta_2\Delta\sigma + \beta_3\bar{\sigma}) \tag{7}$$

and

$$N_i = \left(\frac{\sigma_{eq}}{\sigma_0}\right)^{\alpha} \tag{8}$$

where, $\bar{\sigma}$ and $\Delta\sigma$ are the mean and amplitude of Cauchy stress obtained from finite element calculations, H the Heaviside function, R the loading ratio, and β_1, β_2, β_3 σ_0, α are material parameters to be identified.

It has to be noticed that, due to continuity at $R=0$, β_1, β_2 and β_3 are correlated:

$$\beta_3 + \beta_2 - \beta_1 = 1 \tag{9}$$

Finally, four coefficients have to be identified: β_1, β_2, σ_0 (normative stress), α (power law coefficient).

The model coefficients were identified by adding our experimental database to the one obtained by Andre and using the optimisation package of Zebulon. The optimised set of parameter is the following one: $\beta_1 = 0.98$, $\beta_2 = -1.43$, $\sigma_0 = 1.98$, $\alpha = -2.5$.

5.1.1. Assessment of the criterion

As shown in Fig. 3(b), the model is able to correlate the fatigue lifetime within a factor of 2 scatter bands. It has to be noticed also that the value of β_1 is approximately equal to 1, demonstrating that the maximum stress is the critical variable at $R \leq 0$. Indeed, taking $\beta_1 = 1$ gives:

$$\sigma_{eq} = \Delta\sigma + \bar{\sigma} = \sigma_{max} \quad \text{at } R \leq 0 \tag{10}$$

The conclusion that compressive stresses have no effect on the fatigue lifetime in the range of stresses explored, appears to be fairly established. Nevertheless, it is not possible to extrapolate these results to higher compressive stresses. Indeed, Cadwell [12] has shown that large compressive stresses could damage the material, maybe by involving other physical phenomena (for instance friction under large compressive loadings) than those involved in our case.

5.2. Multiaxial criteria

5.2.1. Invariant based criterion (C_{IBC})

Early multiaxial fatigue life prediction studies [13–15] attempt to correlate the fatigue life to a mean and amplitude quantity of stress (or strain) computed from the first and second stress (or strain) tensor invariant defined by:

$$J_1(\sigma) = \frac{1}{3}\text{Trace}(\sigma) \quad \text{and}$$
$$J_2(\sigma) = \left(\frac{3}{2}\text{Trace}((\sigma')^2)\right)^{(1/2)} \tag{11}$$

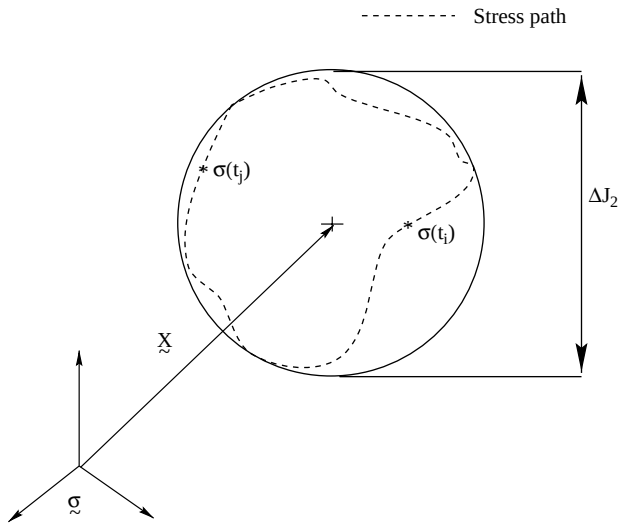

Fig. 4. Representation of the stress amplitude in a 6 dimensional stress state.

Where σ' denotes the deviatoric stress tensor. J_1 is relative to the pressure state whereas J_2 refers to the octahedral shear. J_2 amplitude is defined in the stress space by the geometrical construction shown Fig. 4 (smallest hypersphere including the stress path) which can be reduced to Eq. (12) in simple cases.

$$J_2^* = \frac{\Delta \mathbf{J}_2}{2} = \frac{1}{2} \operatorname*{Max}_{t_i} \left[\operatorname*{Max}_{t_j} [J_2(\underset{\sim}{\sigma}(t_i) - \underset{\sim}{\sigma}(t_j)] \right] \tag{12}$$

In a first approach the uniaxial criteria given Eq. (8) was extended to multiaxial stress states by computing an equivalent stress as a linear combination of the algebraic mean J_1 value and the half J_2 amplitude during a cycle. The criterion can then be expressed as:

$$\sigma_{\text{eq}} = H(-R)\left[J_2^* + \beta_1' \bar{p}\right] + H(R)\left[\beta_2' J_2^* + \beta_3' \bar{p}\right] \tag{13}$$

where H is the Heaviside step function and R the loading ratio. β_1', β_2', β_3' are the material parameters computed from β_1, β_2 and β_3 in order to obtain the same equivalent stress under uniaxial loadings as the one computed using Eq. (7). For multiaxial stress states R has no meaning since neither maximal nor minimal stress can be defined. In this case, the following expression will be preferred (equivalent to Eq. (13) for the uniaxial case):

$$\sigma_{\text{eq}} = \text{Min}\left[\left\langle J_2^* + \beta_1' \bar{p} \right\rangle, \left\langle \beta_2' J_2^* + \beta_3' \bar{p} \right\rangle\right] \tag{14}$$

where $\langle\,\rangle$ denotes the MacCauley bracket (i.e. $\langle x \rangle = 0.5(x + |x|)$). The power low function parameters σ_0 and α are the same as identified previously.

5.3. Critical plane approach (C_{CPA})

As two main mechanisms have to be taken into account (damage and reinforcement), it is proposed to write an equivalent stress as:

$$\sigma_{\text{eq}} = \frac{\Phi_{\text{damage}}}{1 + \Phi_{\text{reinforcement}}} \tag{15}$$

where Φ_{damage} and $\Phi_{\text{reinforcement}}$ are two quantities to be computed from the stress history. The following sections focus on their computation.

5.3.1. Damage modeling: Φ_{damage}

As said previously, in any of the fatigue loadings encountered in this study, cracks were found to initiate on a plane which orientation is given by the direction of the maximum principal stress reached during a cycle: the critical plane (CP). This plane is defined by its normal, $\vec{n}_{\text{CP}}$, which coordinates depend on time due to the material plane rotations under large strain conditions. Since compressive stresses have a negligible effect on fatigue life and NR exhibits tensile crack behaviour, the maximal normal stress acting on the critical plane was considered to control the fatigue damage evolution, say $\sigma_{\vec{n}_{\text{CP}},\max}$. The critical plane is defined as the plane experiencing the maximum principal stress over a cycle. Due to large deformation, special attention has to be given to the difference between stress vectors directions and normals to physical planes. In our case the critical plane is the plane which experiences the maximal normal stress, i.e. the plane on which act the maximum principal stress, $\sigma^P_{\max_t}$ during a cycle. It follows that $\vec{n}_{\text{CP}}$ and the eigen vector $\vec{V}^P_{\max}$ coincide at (and only at) this particular instant $t_{\max}$. Once identified in the deformed configuration, $\vec{n}_{\text{CP}}$ has to be mapped into the undeformed configuration following:

$$\vec{n}_{\text{CP}}^{t_0} = \left(\left(\underset{\sim}{F}^{-1}_{t_{\max}} \right)^T \right)^{-1} \odot \vec{n}_{\text{CP}}^{t_{\max}} \tag{16}$$

where $\underset{\sim}{\mathbf{F}}$ is the transformation gradient and the operator $\odot$ is the so called operator of normalized transport defined by:

$$\frac{\underset{\sim}{T} \odot \vec{u} = \underset{\sim}{T} \cdot \vec{u}}{|\underset{\sim}{T} \cdot \vec{u}|} \tag{17}$$

$\underset{\sim}{T}$ being a tensor and $\vec{u}$ a vector. Then, the normal and shear stress history is rebuilt on the CP as follows:

$$\sigma(t)_{\vec{n}(t)} = (\underset{\sim}{\sigma}(t) \cdot \vec{n}(t)) \cdot \vec{n}(t) \tag{18}$$

$$\tau_{\vec{n}_t} = \sqrt{|\underset{\sim}{\sigma}(t) \cdot \vec{n}(t)|^2 - (\sigma_{n_t})^2} \tag{19}$$

with

$$\vec{n}(t) = \left(\underset{\sim}{\mathbf{F}}^{-1}_t \right)^T \odot \vec{n}_{\text{CP}}^{t_0} \tag{20}$$

5.4. Reinforcement modeling: $\Phi_{reinforcement}$

From observations, we suggest that the reinforcement effect is proportional to the minimum crystallinity level on the CP during a cycle. The evolution of the crystallinity level as a function of the stress was identified using wide angle X-ray scattering (WAXS). An empirical relation was obtained between the crystallization level and the stress applied:

$$X_c(\sigma_{\text{reinf}}) = 0.3(1 - \exp(-D \cdot \langle \sigma_{\text{reinf}} - \sigma_{\text{threshold}} \rangle)) \tag{21}$$

where $\langle\ \rangle$ denotes the MacCauley bracket, σ_{reinf} an equivalent stress describing the reinforcement and $\sigma_{\text{threshold}}$ a threshold value for crystallisation. The asymptotic value of 0.3 refers to the 30% maximal crystallization observed on NR under stretch at room temperature. This result is in agreement with other results published in the literature [16–18]. For uniaxial fatigue tests σ_{reinf} is simply the minimum axial stress reached during a cycle if positive ($R>0$), zero otherwise. For multiaxial loadings the case is more complex. It was proposed that reinforcement occurs as soon as the crack tip does not relax completely during a cycle. It occurs in two cases: when the normal stress on the CP is always positive or when the shear stress on the CP is different from zero at the crack closure (the crack closure corresponds at $\sigma_{\vec{n}_{\text{CP,min}}}=0$). In the later case, even if a compressive stress acts on the critical plane, the shear stress at crack closure $\tau_{\vec{n}_{\text{CP,at crack closure}}}$ prevents the crack tip to relax and allows the cumulative effect of crystallisation to take place. Then, the equivalent stress for reinforcement is computed from the normal and shear stress history on the critical plane as follow:

$$\sigma_{\text{reinf.}} = H\left(\sigma_{\vec{n}_{\text{CP, min}}}\right) * \sqrt{\left(\sigma_{\vec{n}_{\text{CP, min}}}\right)^2 + \left(\tau_{\vec{n},t=t_{\text{min}}}\right)^2} \tag{22}$$

$$+H\left(-\sigma_{\vec{n}_{\text{CP,min}}}\right) * \tau_{\vec{n}_{\text{CP,at crack closure}}} \tag{23}$$

5.4.1. Summary of the fatigue life computation method

The procedure for computing, from the Cauchy stress history, the fatigue life using the C_{CPA} is the following:

Step 1 identification of the critical plane as the plane experiencing the first maximum principal stress over a cycle,

Step 2 mapping the given plane into the undeformed configuration

$$\vec{n}_{\text{CP}}^{\,t_0} = \left(\left(\underset{\sim}{\mathbf{F}}_{t_{\text{max}}}^{-1}\right)^T\right)^{-1} \odot \vec{n}_{\text{CP}}^{\,t_{\text{max}}} \tag{24}$$

Step 3 rebuilding the stress history on the critical plane

$$\sigma(t)_{\vec{n}(t)} = (\underset{\sim}{\sigma}(t)\cdot\vec{n}(t))\cdot\vec{n}(t) \tag{25}$$

$$\tau_{\vec{n}_t} = \sqrt{|\underset{\sim}{\sigma}(t)\cdot\vec{n}(t)|^2 - (\sigma_{n_t})^2} \tag{26}$$

with

$$\vec{n}(t) = \left(\underset{\sim}{\mathbf{F}}_t^{-1}\right)^T \odot \vec{n}_{\text{CP}}^{\,t_0} \tag{27}$$

Step 4 computing the reinforcement and damage quantities

$$\sigma_{\text{reinf.}} = H\left(\sigma_{\vec{n}_{\text{CP,min}}}\right) * \sqrt{\left(\sigma_{\vec{n}_{\text{CP,min}}}\right)^2 + \left(\tau_{\vec{n},t=t_{\text{min}}}\right)^2} \tag{28}$$

$$+H\left(-\sigma_{\vec{n}_{\text{CP,min}}}\right) * \tau_{\vec{n}_{\text{CP,at crack closure}}} \tag{29}$$

$$\Phi_{\text{reinforcement}} = 1 + \xi X_c(\sigma_{\text{reinf}}) \tag{30}$$

$$\Phi_{\text{damage}} = \underset{t}{\text{Max}}\ \sigma_{\vec{n}(t)\text{CP}} \tag{31}$$

Step 5 compute the equivalent stress

$$\sigma_{\text{eq}} = \frac{\Phi_{\text{damage}}}{1+\Phi_{\text{reinforcement}}} \tag{33}$$

Step 6 compute the fatigue life

$$N_i = \left(\frac{\sigma_{\text{eq}}}{\sigma_0}\right)^{\alpha} \tag{34}$$

The material parameters for the model are ξ, D and $\sigma_{\text{threshold}}$, σ_0 and α. The value of N_i is calculated using a power law function as proposed previously.

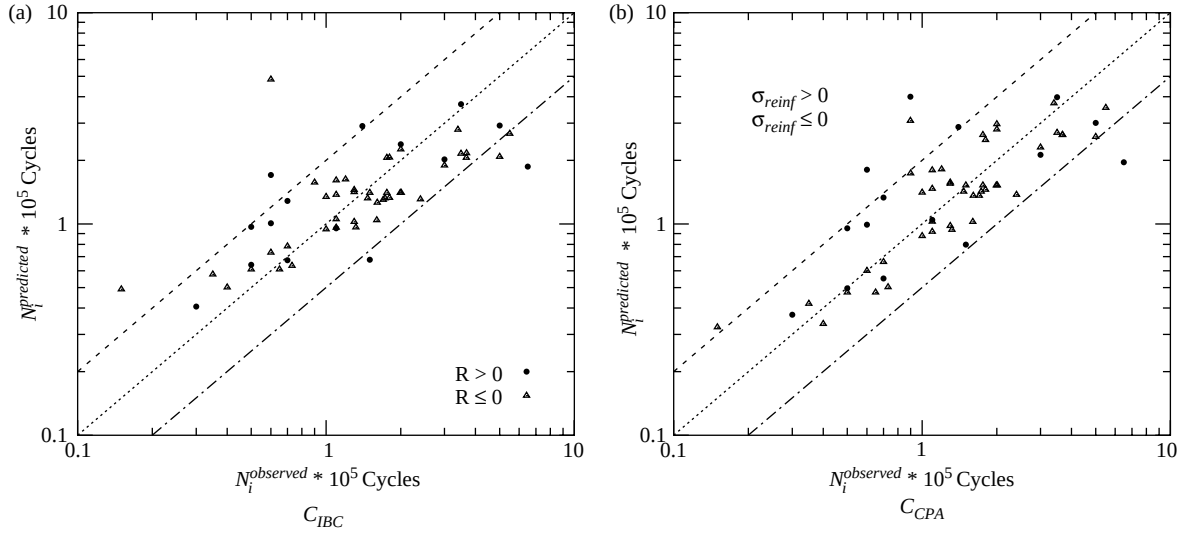

Fig. 5. Scatter obtained on uniaxial tests after material constants identification for C_{IBC} and C_{CPA} criteria. Dashed lines represent a factor of two scatter bands.

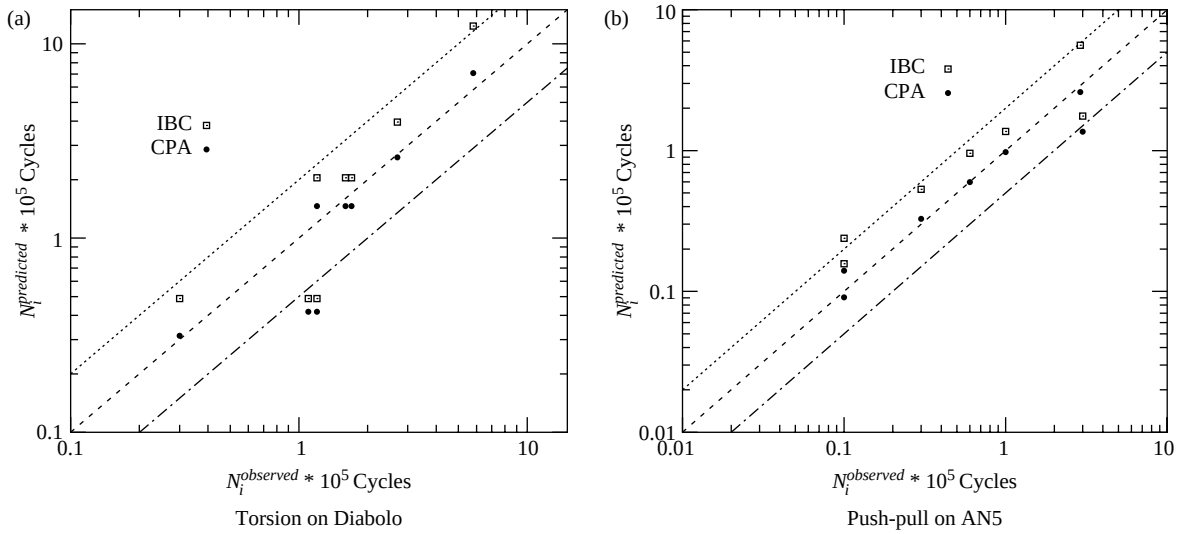

Fig. 6. Comparison between predicted and observed lives for C_{IBC} and C_{CPA} criteria.

5.5. Material parameters identification

The criterion was implemented in the C++ object oriented FE code ZeBuLoN. The optimization loop was driven by the optimization package of ZeBuLoN, using genetic evolutionary algorithm [19] and the whole uniaxial fatigue data base. The following set of parameters was obtained, $\xi = 7.3$, $D = 0.62$, $\sigma_{\mathrm{threshold}} = 0.17$ MPa, $\sigma_0 = 2$ MPa, $\alpha = -2.88$.

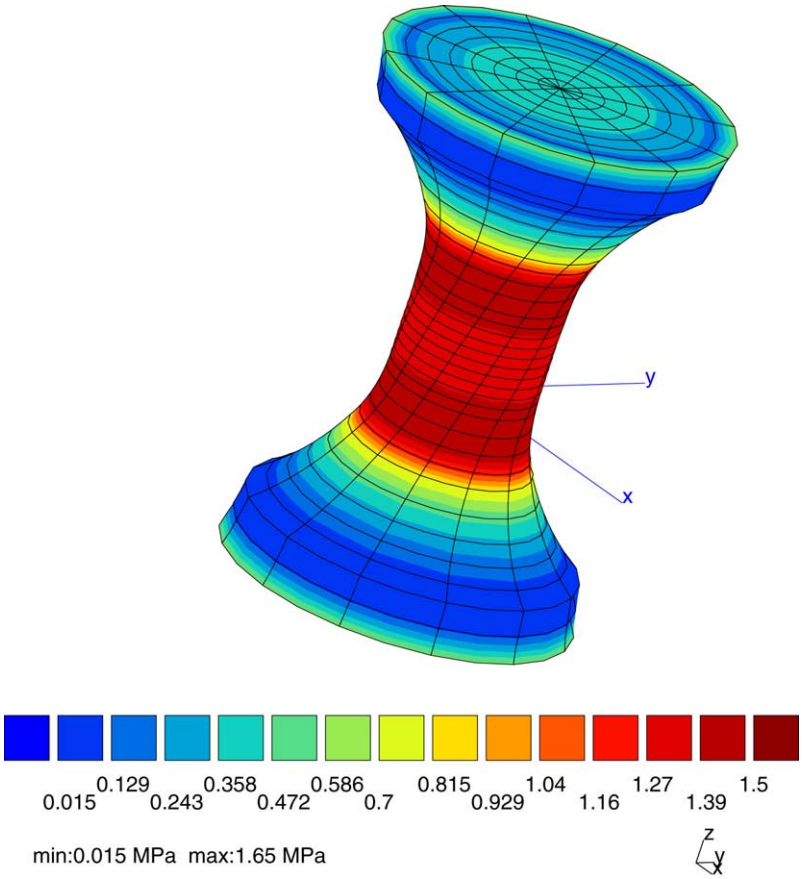

Fig. 7. 3D FE computation for a Diabolo under 60° static torsion and tension-compression. Mesh and first principal stress map in deformed configuration (60°, axial load 600 N).

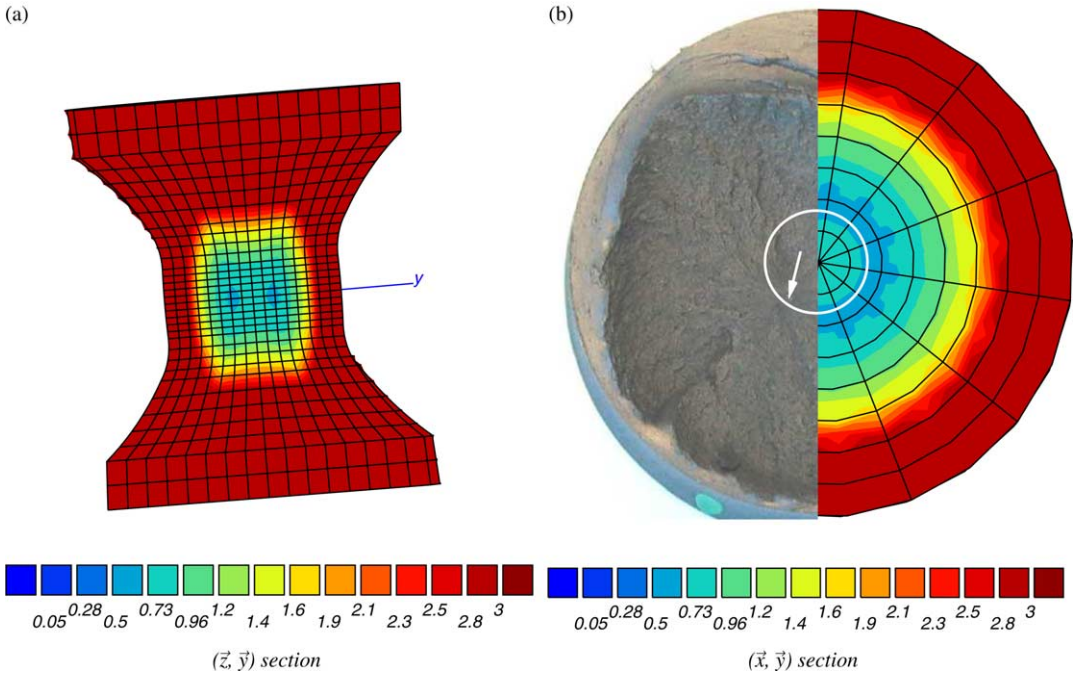

Fig. 8. C_{CPA} results for static torsion and tension compression test on a Diabolo specimen (60°, cyclic axial load ± 600 N). Predicted fatigue lives contour maps (in 10^5 cycles) and comparison to experimentally observed crack location (the arrow shows the crack initiation location).

6. Results

6.1. Uniaxial results

Uniaxial results are presented Fig. 5 for C_{IBC} and C_{CPA} criteria in a log log plot of the predicted versus observed fatigue lifes. Both criteria give good results with a scatter slightly greater for the C_{IBC} than for the C_{CPA}.

6.2. Multiaxial results

6.2.1. C_{IBC} and C_{CPA} comparison

Fig. 6 summarizes the comparison between observed and predicted lives for torsion tests on Diabolo and tension-compression on AN5. First, C_{IBC} results are systematically above C_{CPA} predictions. For Torsion tests on Diabolo, this difference is lower than for push–pull on AN5. Fatigue test results on AN2 specimens (not shown) show the same trend. The most critical point is that C_{IBC} calculations result in non-conservative predictions. The fairly good agreement between predicted and observed lives using C_{CPA} strongly suggests that this approach has to be preferred. Moreover, C_{CPA} has been found to predict precisely the fatigue crack orientation [21], which gives a strong support to the theory. To explain the differences observed between C_{IBC} and C_{CPA}, stress states under torsion and push–pull have to be considered in terms of deviatoric and hydrostatic part. C_{IBC} considers separately the deviatoric and hydrostatic parts of the stress tensor contrary to C_{CPA}. The stress amplitude is computed using the deviatoric part whereas the hydrostatic part represents the mean stress

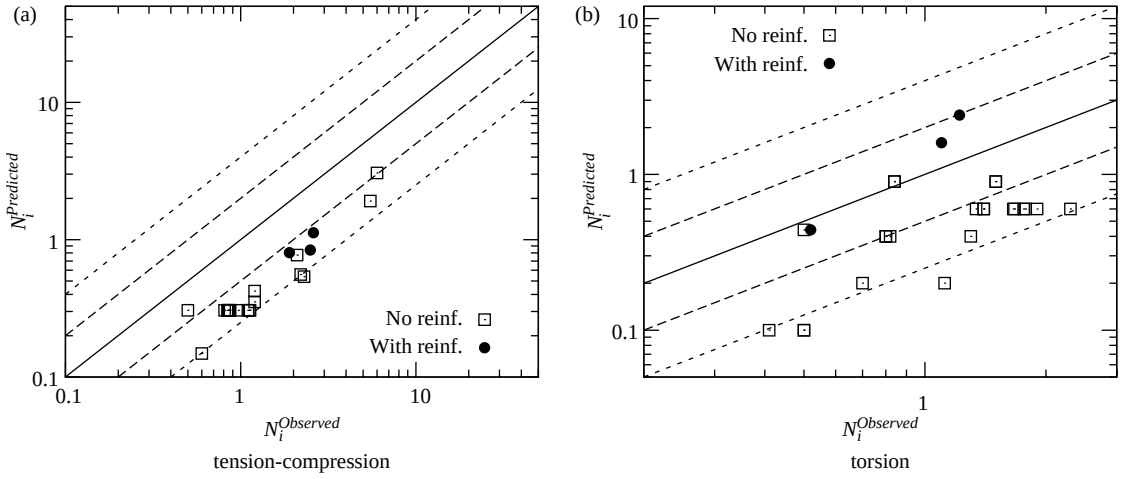

Fig. 9. Scatter obtained with the C_{CPA} criteria applied to tension-compression and torsion tests on AN2 specimens. Fatigue lives in 10^5 cycles.

effect. Under torsion, the stress state is mainly a deviatoric stress state (not completely deviatoric due to large strains). As a consequence the amplitude term is far larger than the mean stress term and no reinforcement can be taken into account. On the contrary, the stress state at the notch of a AN5 under tension shows relatively high triaxiality levels so that the deviatoric part becomes negligible compared to the hydrostatic part. Hence, for most fatigue tests on AN5, the mean hydrostatic stress is larger than the deviatoric stress amplitude and a reinforcing effect is predicted whatever the applied loading ratio. Moreover, and this is probably the most problematic aspect of such a criteria, infinite fatigue life is predicted by C_{IBC} under purely hydrostatic stress state whereas finite fatigue life is observed experimentally [20]. Indeed, in this particular case $J_2=0$ which makes the equivalent stress to be systematically equal to zero (i.e. infinite life). By nature, C_{CPA} has not such a behaviour depending on the triaxiality ratio. In the following, only the C_{CPA} will be considered.

6.2.2. Static torsion and push–pull results

Static torsion and push–pull fatigue tests on Diabolos are of particular interest since they show systematical internal crack initiation. However the crack initiation plane was quasi-normal to the specimen axis (less than 5° off the specimen axis) as observed for simple tension-compression tests. Only the crack inititation location differs. 3D FE computation was performed and the C_{CPA} criteria applied at each node of the mesh so that a full mapping of the fatigue lives within the specimen was obtained. The mesh used (2100 elements, 20 nodes quadratic elements) and a fist principal stress isocontour map is given Fig. 7. Fig. 8 shows the predicted fatigue lives in a diabolo section along $((\vec{z},\vec{y})$ section) and normally $((\vec{x},\vec{y})$ section) to the specimen axis (non-deformed configuration for more clarity) and compare it to the experimentally observed fatigue lives. The fatigue crack initiation location corresponds to the point where the fatigue life is the lowest within the specimen. As shown Fig. 8(b), the predicted and experimental crack location does match. The predicted crack orientation matched the experimental crack plane (not shown). The static torsion induces a permanent shear stress to act on the plane normal to the specimen axis (i.e. the crack initiation plane). Let us describe in detail this particular stress state. The maximum first principal stress direction, which gives the critical plane, is only slightly affected (5°) by the applied static torsion and is close to what it would be if no static torsion was applied. It is then understandable to observe an experimental crack plane quasi-normal to the tensile direction. However, due to the torsion, Φ_{damage} is maximum at the specimen surface and minimum on the specimen axis. The reason why the predicted crack initiation is internal is more complex. For such tests, the equivalent stress for reinforcement is reduced to the shear at the crack closure, which is equal to the shear stress induced by the static torsion. Let us consider the evolution of the different quantities along a segment perpendicular to the specimen axis. The shear stress is equal to zero on the specimen axis and maximum at the specimen surface (around 0.7 MPa in this particular case) so that it cross the critical value for reinforcement ($\sigma_{\mathrm{threshold}}=0.17$ MPa) at a given distance δ from the specimen axis. Φ_{reinf} is equal to zero up to δ, then slowly increase up to its maximum at the specimen surface. The increase in the reinforcement quantity overcome the slow increase of Φ_{damage} so that the minimum equivalent stress is found at the distance δ, and internal failure is predicted.

6.2.3. Tension-compression and torsion tests

Fig. 9 illustrates the scatter obtained on AN2 specimens under tension-compression and torsion. Two main

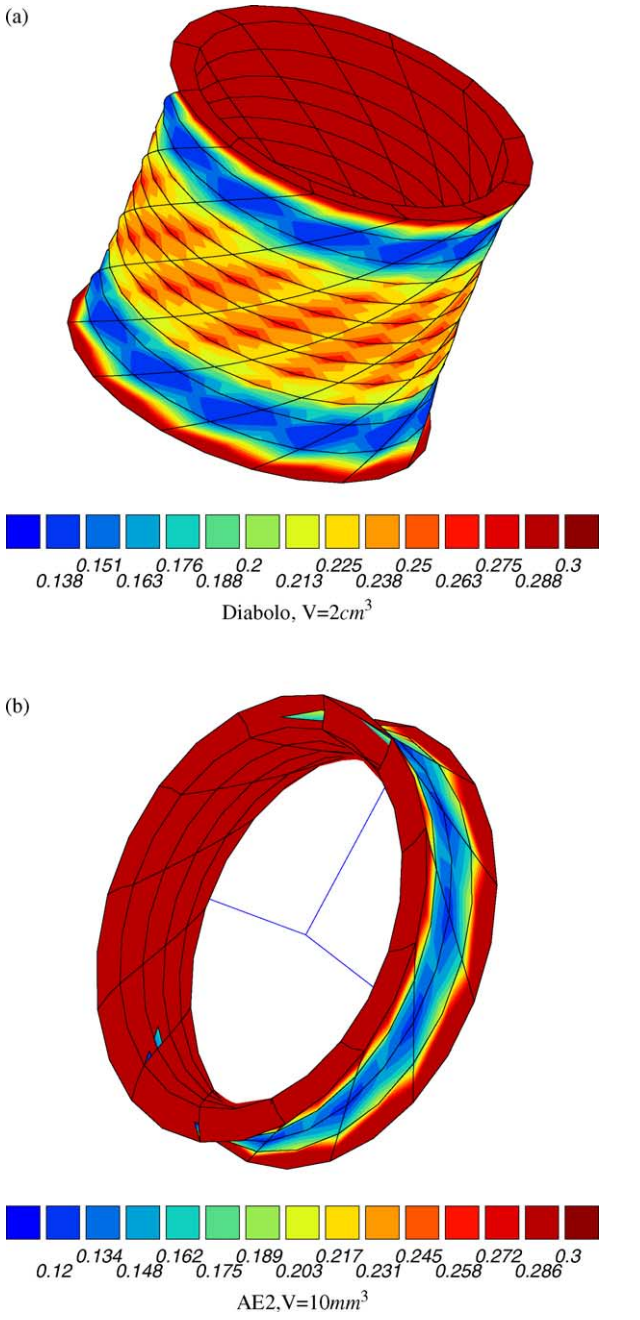

Fig. 10. Volumes where the predicted fatigue life is smaller than three times the predicted fatigue life for a Diabolo specimen and an AN2 specimen under torsion.

observations can be done: the scatter of the results is larger than the one observed for Diabolo specimens and the criterion C_{CPA} is conservative. AN2 specimens show the smallest radius among the notched geometries an such show the strongest gradients. Fig. 10 illustrates the volumes where the predicted fatigue life is smaller than three time the minimum fatigue life for a Diabolo specimen and an AN2 specimen under torsion. In both cases the predicted fatigue lives are the same. It shows that the equally stressed volumes are 200 times smaller on an AN2 than on a Diabolo. Moreover it has to be noticed that the loading with the strongest gradient (torsion) exhibit the largest scatter. It is believed that the differences observed between predicted and observed fatigue lives are due to size and/or gradient effects. Since the proposed criteria uses a local definition of stress, it is not expected to account for volumetric related effects such as gradient and/or size effects. The influence of notches on fatigue lives are well know on metallic materials. Those results seem to show that the same effects can be observed on non-metallic materials such as rubber.

7. Conclusions

Two criteria have been considered for fatigue life prediction under non-proportional multiaxial loadings of rubbery materials. The first one based on the first and second stress invariant of the Cauchy stress tensor is an extension to multiaxial stress states of a previously proposed simple uniaxial criteria. The second one is a new approach based on the critical plane concept. It includes a description of damage end reinforcement mechanisms and thus propose micro to macro approach for fatigue of rubbers. It was found that the first approach was unable to predict correctly the fatigue life, even in simple multiaxial cases such as torsion. The second proposal C_{CPA} is able to predict the fatigue life, locate the crack initiation and orientation for most of the loading encountered in this study. In particular, C_{CPA} is able to predict internal crack initiation for tension-compression with a superimposed static torsion, as observed experimentally. The limitation of the approach is that being computed from local stress values (i.e. at one point) it is unable to account for size or gradient effects as observed on the most notched specimens. Further test have to be performed in order to extend the fatigue data base to more non-proportional stress states (combined tension torsion, in and out of phase) in order to estimate the ability of the proposed criteria in those cases. A new approach is under development to take into account the size/gradient effects.

Acknowledgements

This work was done with the financial support of Paulstra-Hutchinson.

References

[1] Lindley PB. Relation between hysteresis and the dynamic crack growth resistance of natural rubber. Int J Fract 1973;9:449–62.

[2] Rivlin R, Thomas A. Rupture of rubber part 1: characteristic energy for tearing. J Polym Sci 1953;10:291–318.

[3] Griffith AA. The phenomenon of rupture and flow in solids. Philos Trans R Soc London 1920;221:163.

[4] Mars W, Fatemi A. A literature survey on fatigue analysis approaches for rubber. Int J Fatigue 2002;24:949–61.

[5] Saintier N. Multiaxial fatigue life of a natural rubber: crack initiation mechanisms and local fatigue life criterion, PhD dissertation, Ecole des Mines de Paris; 2001.

[6] André N. Critère local d'amorage de fissures en fatigue dans un élastomère de type nr. Thèse Ecole Nationale Supérieure des Mines de Paris; 1997.

[7] Mullins L. Effect of streching on the properties of rubber. J Rubber Res 1947;16:275–89.

[8] Laiarinandrasana L, Piques R, Robisson A. Visco-hyperelastic model with internal state variable coupled with discontinuous damage concept under total lagrangian formulation. Int J Plast 2003;19(7):977–1000.

[9] ZeBuLoN, User manual, Transvalor/ENSMP—Centre des matériaux, BP87 F-91003 Evry Cedex, http://www.mat.ensmp.fr.

[10] Lake GJ. Mechanical fatigue of rubber. Rubber Chem Technol 1971;45: 309–28.

[11] Lake GJ. Fatigue and fracture of elastomers. Int J Fract 1995;68:435–58.

[12] Cadwell SM, Merril RA, Sloman CM, Yost FL. Dynamic fatigue life of rubber. Ind Eng Chem 1940;12:19–23.

[13] Marin J. Interpretation of fatigue strengths for combined stresses. In: Proceedings of the international conference on fatigue of metals. London: Institution of Mechanical Engineers; 1956. p. 184–94.

[14] Sines G. Behavior of metals under complex static and alternating stresses. New York: McGraw-Hill; 1959. p. 145–69.

[15] Crossland B. Effect of large hydrostatic pressure on the torsional fatigue strengh of an alloy steel. In: International conference on fatigue of metals London. London; 1959. p. 138–49.

[16] Alexander L, Ohlberg S, Russell-Taylor G. J Appl Polym Sci 1955;26: 1068.

[17] Lee D, Dononvan J. Microstructural changes in the crack tip region of carbon black filled natural rubber. Rubber Chem Technol 1987;60: 910–24.

[18] Flory P. Thermodynamics of crystallization in high polymers. 1. Crystallization induced by streching. J Chem Phys 1947;15:397.

[19] Goldberg D. Algorithms in search, optimization and machin learning. Reading, MA: Addison-Wesley; 1989.

[20] Gent AN, Lindley PB. Internal rupture of bonded rubber cylinders in tension. Proc R Soc A 1958;246:195–205.

[21] Saintier N, Piques R, Cailletaud G. Crack initiation and propagation under multiaxial fatigue in a natural rubber. Int J Fatigue 2006;28(1):61–72.